Inorganic Chemistry

Article

pubs.acs.org/IC

Cu^{2+} in Layered Compounds: Origin of the Compressed Geometry in the Model System $K_2ZnF_4:Cu^{2+}$

J. A. Aramburu,*[,†] J. M. García-Lastra,[‡] P. García-Fernández,[†] M. T. Barriuso,[§] and M. Moreno[†]

[†]Departamento de Ciencias de la Tierra y Física de la Materia Condensada, Universidad de Cantabria, Avenida de los Castros s/n, 39005 Santander, Spain

[‡]Center for Atomic-Scale Materials Design, Department of Physics, Technical University of Denmark, DK-2800 Kongens Lyngby, Denmark

[§]Departamento de Física Moderna, Universidad de Cantabria, Avenida de los Castros s/n, 39005 Santander, Spain

ABSTRACT: Many relevant properties (including superconductivity and colossal magnetoresistance) of layered materials containing Cu^{2+}, Ag^{2+}, or Mn^{3+} ions are commonly related to the Jahn−Teller instability. Along this line, the properties of the CuF_6^{4-} complex in the K_2ZnF_4 layered perovskite have recently been analyzed using a parametrized Jahn−Teller model with an imposed strain [Reinen, D. *Inorg. Chem.* **2012**, *51*, 4458]. Here, we present results of *ab initio* periodic supercell and cluster calculations on $K_2ZnF_4:Cu^{2+}$, showing unequivocally that the actual origin of the unusual compressed geometry of the CuF_6^{4-} complex along the crystal *c* axis in that tetragonal lattice is due to the presence of an electric field due to the crystal surrounding the impurity. Our calculations closely reproduce the experimental optical spectrum. The calculated values of the equilibrium equatorial and axial Cu^{2+}−F^- distances are, respectively, R_{ax} = 193 pm and R_{eq} = 204 pm, and so the calculated distortion $R_{ax} - R_{eq}$ = 11 pm is three times smaller than the *estimated* through the parametrized Jahn−Teller model. As a salient feature, we find that if the CuF_6^{4-} complex would assume a perfect octahedral geometry ($R_{ax} = R_{eq}$ = 203 pm) the antibonding $a_{1g}^*(\sim 3z^2 - r^2)$ orbital is placed above $b_{1g}^*(\sim x^2 - y^2)$ with a transition energy $E(^2A_{1g} \rightarrow {}^2B_{1g})$ = 0.34 eV. This surprising fact stresses that about half the experimental value $E(^2A_{1g} \rightarrow {}^2B_{1g})$ = 0.70 eV is not due to the small shortening of the axial Cu^{2+}−F^- distance, but it comes from the electric field, $\mathbf{E}_R(\mathbf{r})$, created by the rest of the lattice ions on the CuF_6^{4-} complex. This internal field, displaying tetragonal symmetry, is thus responsible for the compressed geometry in $K_2ZnF_4:Cu^{2+}$ and the lack of symmetry breaking behind the ligand relaxation. Moreover, we show that the electronic energy gain in this process comes from bonding orbitals and not from antibonding ones. The present results underline the key role played by *ab initio* calculations for unveiling all the complexity behind the properties of the model system $K_2ZnF_4:Cu^{2+}$, opening at the same time a window for improving our knowledge on d^9, d^7, or d^4 ions in other layered compounds.

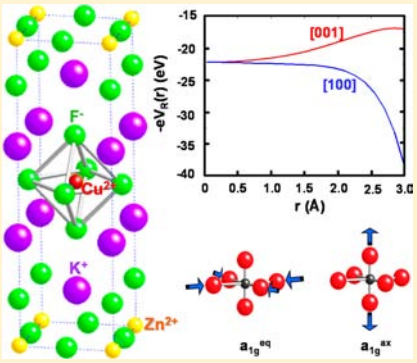

1. INTRODUCTION

A main goal in the investigation of materials is to gain a better insight into the actual origin of its structure, paying special attention to the connection between the arrangement of electronic levels and the equilibrium geometry. In this way, *tiny* changes in the electronic structure are responsible for the tetragonal symmetry of $KMnF_3$,[1] while $KMgF_3$ and $KNiF_3$ perovskites are cubic.[2] Similarly, small variations in the electronic density[3] between $CuCl_4(NH_3)_2^{2-}$ and $CuCl_4(H_2O)_2^{2-}$ complexes, formed in Cu^{2+}-doped NH_4Cl, explain why the former complex is tetragonal[4−6] while the latter one is orthorhombic.[4,5]

In the realm of insulators containing transition metal impurities, significant research has been focused on cubic *halide* lattices doped with d^9 ions such as Cu^{2+}, Ag^{2+}, or Ni^+.[7−10] In all cases explored *up to now* Electron Paramagnetic Resonance (EPR) data undoubtedly prove that the impurity centers have tetragonal D_{4h} symmetry with the unpaired electron placed in the antibonding $b_{1g}^*(\sim x^2 - y^2)$ orbital, and thus a $^2B_{1g}$ ground state. In cubic material such as the $CsCdF_3$ perovskite, this fact *necessarily* means that the local equilibrium geometry corresponds to an elongated octahedron as a result of a static Jahn−Teller (JT) effect where four equatorial ligands are lying at a distance, R_{eq}^0, from the impurity while two axial ligands are at $R_{ax}^0 > R_{eq}^0$.[7,8] Bearing these relevant data in mind, the experimental results obtained for the Cu^{2+}-doped tetragonal layered perovskite K_2ZnF_4 (Figure 1) are certainly surprising.[11−13] Indeed the *g*-tensor of $K_2ZnF_4:Cu^{2+}$ measured by EPR at T = 6 K has axial symmetry with the crystal *c* axis as the principal axis and the values $g_{\parallel}$ = 2.003 and $g_{\perp}$ = 2.386.[12] These values clearly prove that the unpaired electron of the CuF_6^{4-} complex is lying in the antibonding $a_{1g}^*(\sim 3z^2 - r^2)$ orbital (Figure 2), and thus the electronic ground state is $^2A_{1g}$. At the same time, they strongly suggest that the fluorine octahedron around a Cu^{2+} impurity is axially compressed and not elongated.

Received: January 15, 2013
Published: May 31, 2013

   dx.doi.org/10.1021/ic400105z | *Inorg. Chem.* 2013, 52, 6923−6933

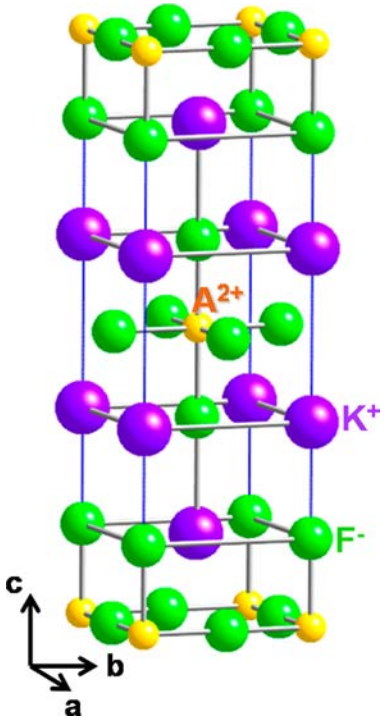

Figure 1. Unit cell of K_2AF_4 (A = Mg, Zn) layered perovskites.

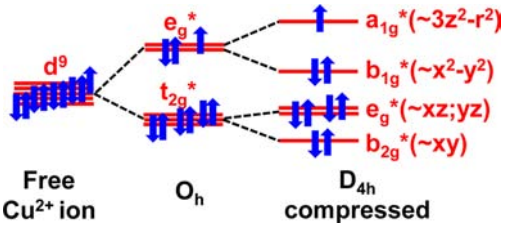

Figure 2. Qualitative description of the splitting of d-levels of a Cu^{2+} ion, first under an octahedral (O_h) environment and then after a distortion giving rise to a tetragonal (D_{4h}) compressed geometry.

An attempt to describe this unexpected situation found in K_2ZnF_4:Cu^{2+} has been carried out by means of a *parametrized* JT model where the involved parameters are fitted to available experimental data.[11,15] Nevertheless, this parametrized model is unable to answer a fundamental question: why precisely in K_2ZnF_4:Cu^{2+} the local geometry around Cu^{2+} impurities is tetragonally compressed and not elongated like it is found in Cu^{2+}-doped $CsCdF_3$ or $KZnF_3$ lattices.[9,10,14] Moreover, the use of a JT model for explaining the experimental data on K_2ZnF_4:Cu^{2+} is not necessarily appropriate. Indeed, the existence of a JT effect requires a *departure point* where the local symmetry is *cubic* and the two $b_{1g}^*(\sim x^2 - y^2)$ and $a_{1g}^*(\sim 3z^2 - r^2)$ levels are thus degenerate.[8,16] Although the K_2ZnF_4 lattice is tetragonal it is true that the equatorial (R_{eq}^H = 202.9 pm) and axial (R_{ax}^H = 202.6 pm) Zn^{2+}−F^- distances of the host lattice are practically equal,[17] and thus it can be thought that when Zn^{2+} is replaced by Cu^{2+}, this impurity observes a local cubic symmetry before the distortion comes out. Nevertheless, the axial F^- ligands in K_2ZnF_4, which are along the crystal *c* axis, have a terminal character whereas the equatorial ones are bridging two close Zn^{2+} ions (Figure 1). For this reason, it can be expected that the force constant for moving an equatorial ligand along the metal−ligand distance, K_{eq}, will be higher than that corresponding to an axial ligand, K_{ax},[18] thus outlining that the local geometry cannot in fact be considered as cubic.

Similar situations can be found in a large number of compounds, and in many cases, the geometrical configuration of the system is attributed to the JT effect *without* a proper critical analysis. Therefore, it is of great importance to carefully determine the origin of the geometry of the system. This is particularly true as some of these systems are materials with a strong technological importance like high-temperature superconductors or layered manganites displaying colossal magnetoresistance.[19−23]

Furthermore, *ab initio* cluster calculations performed on a CuF_6^{4-} complex embedded in the layered perovskite K_2MgF_4, which is isomorphous to K_2ZnF_4,[24,2] point out that *even when* the axial, R_{ax}, and equatorial, R_{eq}, distances are equal, the two $b_{1g}^*(\sim x^2 - y^2)$ and $a_{1g}^*(\sim 3z^2 - r^2)$ levels are surprisingly *not degenerate*.[25] However, the validity of results derived from cluster calculations for Cu^{2+}-doped K_2AF_4 (A = Zn, Mg) has recently been questioned,[15] arguing that the environment extends to infinity, and thus an exact treatment must take the lattice periodicity into account.

Bearing all these facts in mind, the present work is aimed at reaching a true microscopic understanding of the local geometry in K_2ZnF_4:Cu^{2+} by means of first principle calculations. Moreover, due to its relative simplicity, K_2ZnF_4:Cu^{2+} is a perfect model system to gain a better insight into the properties of d^9, d^4, and d^7 ions in layered compounds. Particular attention is paid in this work to determine whether the ligand relaxation around a Cu^{2+} impurity can or cannot be properly explained as a result of a JT effect. For achieving this goal, large periodic supercells are used in a first step for calculating R_{ax}^0 and R_{eq}^0 values in K_2ZnF_4:Cu^{2+}. For comparison purposes, similar calculations are also performed on *closed shell* impurities like Cd^{2+} or Be^{2+} in K_2ZnF_4 and K_2MgF_4. For the same reason, the equilibrium geometries of divalent transition metal impurities Mn^{2+} and Ni^{2+} in the same host lattices[26−28] are explored by means of periodic supercells calculations. These impurities are known to induce only a fully isotropic ligand relaxation in cubic perovskites like $KMgF_3$ or $CsCaF_3$.[29]

Seeking to understand the mechanisms responsible for the equilibrium geometry in K_2ZnF_4:Cu^{2+}, how the electronic levels are arranged at the equilibrium geometry, described by R_{ax}^0 and R_{eq}^0 distances, and also when $R_{ax} = R_{eq}$, is explored in a second step. To test the reliability of conclusions, the calculated value of $^2A_{1g} \rightarrow {}^2B_{1g}$, $^2A_{1g} \rightarrow {}^2E_g$, and $^2A_{1g} \rightarrow {}^2B_{2g}$ electronic transitions at the equilibrium geometry are compared with optical absorption data obtained on K_2ZnF_4:Cu^{2+}.[13,14]

This work is arranged as follows. In section 2, an account of methods employed for performing *ab initio* calculations is provided. For the sake of clarity, a brief recall on the JT effect is given in section 3, while main results are presented and discussed in section 4. Finally, some remarks are included in the last section.

2. COMPUTATIONAL DETAILS

Geometry optimizations on periodic supercells simulating diluted M impurities (M = Cu^{2+}, Mn^{2+}, Ni^{2+}, Cd^{2+}, and Be^{2+}) doped in K_2ZnF_4[17] and K_2MgF_4[24] lattices (tetragonal *I*4/*mmm* space group) have been performed by means of the CRYSTAL (version 09) code[30] under the framework of Density Functional Theory (DFT). Most of the calculations were performed using 2 × 2 × 1 periodic supercells containing 56 atoms. In order to be sure that impurity−impurity interactions between supercells are negligible, some calculations were repeated on 3 × 3 × 1 supercells (126 atoms), and the results were

dx.doi.org/10.1021/ic400105z | Inorg. Chem. 2013, 52, 6923−6933

practically unmodified. In the CRYSTAL code, the Bloch wave functions are represented by a linear combination of atomic orbitals which, in turn, are expressed as a combination of Gaussian basis functions. All ions have been described by means of all-electron basis sets taken directly from CRYSTAL's web page;[30] in particular, we have used the following bases: 86-4111(41D)G_doll_2000 for Cu, 86-511G_dovesi_1991 for K, 86-411d31G_jaffe_1993 for Zn, 8-511d1G_valenzano_2006 for Mg, and 7-311G_nada_1993 for F. Following previous works, we have used the B1WC hybrid exchange-correlation functional (including 16% of Hartree−Fock exchange)[31] that does not require the input of any semiempirical parameter particular to the system and has shown to be able to reproduce with great accuracy the geometry and properties of a large number of both pure and doped crystals. The integration in reciprocal space was carried out by sampling the Brillouin zone with the 4 × 4 × 8 Monkhorst−Pack net, which is enough to provide a full energy convergence.

As the ability of the CRYSTAL program to treat excited states is limited, we have calculated the energies of the d−d electronic transitions of the $K_2ZnF_4:Cu^{2+}$ through the usual ΔSCF approach by means of the Amsterdam density functional (ADF) code[32] that allows performing DFT calculations on each specific electronic configuration. Impurity centers are calculated in the ADF code through the cluster approach taking into account the electrostatic potential created by the rest of the infinite crystal lattice ions on the cluster. In these calculations, 37 atom clusters were used in conjunction with the popular B3LYP hybrid functional[33] in the spin-unrestricted Kohn−Sham formalism of the DFT. The use of finite clusters for describing the properties of these centers is consistent with the highly localized character of the unpaired electrons residing essentially in the CuF_6^{4-} complex region. In addition, such as will be later seen, the equilibrium geometries calculated through the cluster approximation for all systems analyzed in this work are very similar to those obtained in the periodic calculations. We have used high-quality all-electron basis sets of the triple-ζ plus polarization (TZP) type formed of localized Slater-type functions as implemented in the 2012.01 version of the ADF code.[32] The electrostatic potential from the rest of the lattice ions was generated by means of 250 point charges with values previously fitted to reproduce the electric field corresponding to the infinite system.[34,35]

3. RECALL ON THE JAHN−TELLER EFFECT

When an impurity like Mn^{2+} enters a *cubic* perovskite like $CsCdF_3$ replacing Cd^{2+}, it produces an *isotropic* relaxation of six ligands.[29] This makes that the impurity-ligand distance, R, has an equilibrium value equal to R^*, different from the $Cd^{2+}-F^-$ distance of the perfect lattice, R^H, but the local symmetry remains cubic. This process is the result of the coupling of the orbitally singlet $^6A_1(t_{2g}^3e_g^2)$ ground state only with the symmetric vibrational mode, a_{1g}, of the MnF_6^{4-} complex. However for d^9 ions in cubic crystals and octahedral coordination, the electronic ground state, ^2E_g, is orbitally degenerate (Figure 2) leading to an *additional* relaxation mechanism involving the nonsymmetric e_g mode.[7,8] Therefore, the ^2E_g state is linearly coupled to *both* a_{1g} and e_g modes through the H_v Hamiltonian given by[16]

$$H_v = H_v^a + H_v^e; \qquad H_v^a = V_a(\mathbf{r})Q_a;$$
$$H_v^e = V_\theta(\mathbf{r})Q_\theta + V_\varepsilon(\mathbf{r})Q_\varepsilon \tag{1}$$

Here, the normal coordinate Q_a is proportional to $(R - R^H)$, while $V_\theta(\mathbf{r})$ and Q_θ both transform like $3z^2 - r^2$, and $V_\varepsilon(\mathbf{r})$ and Q_ε like $x^2 - y^2$. If, only under the influence of H_v^a, $R_{ax} = R_{eq} = R^*$, then the subsequent action of H_v^e gives rise to adiabatic minima displaying tetragonal symmetry with a principal axis which can be one of the three C_4 axes of the crystal. For instance, a tetragonal distortion described by $Q_\theta \neq 0$, $Q_\varepsilon = 0$ is

$$R_{ax} - R^* = -2(R_{eq} - R^*) = 2\eta;\ Q_\theta = -\sqrt{12}\,\eta \tag{2}$$

The equivalence among the three possible distortions is, however, destroyed by random strains, inevitably present in any real crystal,[36] which favors one of the three C_4 axes of the octahedron as being the principal axis of a *local* D_{4h} symmetry. These facts are responsible for the observation, at low temperatures, of *tetragonal* EPR spectra due to d^9 ions in cubic crystals,[7,8,36] characterized by two different gyromagnetic factors, $g_\parallel$ and $g_\perp$. This is the fingerprint of a static JT effect involving symmetry breaking where three types of centers are simultaneously observed making the whole system optically isotropic. A temperature raising favors rapid reorientations among the three possible distortions leading to an isotropic EPR spectrum characterized by $g = (g_\parallel + 2g_\perp)/3$.[7,8,36] Nevertheless, in a few cases, like $MgO:Cu^{2+}$ or $MgO:Ag^{2+}$, the low temperature EPR spectra exhibit a *cubic* angular pattern reflecting the existence of *coherent* tunneling among the three possible distortions.[36−38] The conditions for observing this unusual behavior are discussed in refs 39 and 40.

From eq 3, if we have an impurity in a cubic crystal with an orbitally singlet state described by $|\Psi_g\rangle$, then symmetry rules imply $\langle\Psi_g|V_\theta(r)|\Psi_g\rangle = 0$. As the ground state of a d^9 ion in a cubic perovskite can be viewed as a closed shell and three electrons in the antibonding e_g^* open shell, the only nonzero contribution to $\langle\Psi_g|V_\theta(r)|\Psi_g\rangle$ comes from such electrons. According to the center-of-gravity theorem[41] $\langle x^2 - y^2|V_\theta(\mathbf{r})|x^2 - y^2\rangle$ and $\langle 3z^2 - r^2|V_\theta(\mathbf{r})|3z^2 - r^2\rangle$ matrix elements are *not independent* but verify

$$\begin{aligned}\langle x^2 - y^2|V_\theta(\mathbf{r})|x^2 - y^2\rangle &= -\langle 3z^2 - r^2|V_\theta(\mathbf{r})|3z^2 - r^2\rangle \\ &= V_{1e}\end{aligned} \tag{3}$$

The energy change of $b_{1g}^*(\sim x^2 - y^2)$ and $a_{1g}^*(\sim 3z^2 - r^2)$ orbitals due to H_v^e, when $Q_\varepsilon = 0$, can be written as a function of the vibronic constant, V_{1e}, and the Q_θ coordinate as

$$\delta\varepsilon(3z^2 - r^2) = -V_{1e}Q_\theta;\ \delta\varepsilon(x^2 - y^2) = V_{1e}Q_\theta \tag{4}$$

Therefore, if $n(x^2 - y^2)$ and $n(3z^2 - r^2)$ denote the number of electrons in the corresponding orbitals, the total energy variation due only to the H_v^e term, ΔE_v^e, is equal to

$$\begin{aligned}\Delta E_v^e &= n(3z^2 - r^2)\delta\varepsilon(3z^2 - r^2) + n(x^2 - y^2)\delta\varepsilon(x^2 - y^2) \\ &= \delta\varepsilon(3z^2 - r^2)\{n(3z^2 - r^2) - n(x^2 - y^2)\}\end{aligned} \tag{5}$$

Accordingly, a kind of stable distortion, characterized by Q_θ^0 (and $Q_\varepsilon^0 = 0$) requires that

$$\Delta E_v^e(Q_\theta^0) < 0 \tag{6}$$

Nevertheless, for obtaining the final energy shift, E_{JT}, conveyed by the distortion, it is necessary to add the increase of elastic energy associated with the distortion[8,36,16] and then

$$\begin{aligned}E_{JT} &= (1/2)\Delta E_v^e(Q_\theta^0) \\ &= (1/2)\delta\varepsilon(3z^2 - r^2)\{n(3z^2 - r^2) - n(x^2 - y^2)\}\end{aligned} \tag{7}$$

Therefore, in a static JT effect the necessary energy decrease ($E_{JT} < 0$) associated with the distortion comes *only* from the different population of antibonding $b_{1g}^*(\sim x^2 - y^2)$ and

dx.doi.org/10.1021/ic400105z | Inorg. Chem. 2013, 52, 6923−6933

a_{1g}*($\sim 3z^2 - r^2$) levels, and thus bonding orbitals, belonging to closed shells, do not contribute to the stabilization (Figure 2).

The R* value for d^9 ions can be obtained from calculations on the $(3z^2 - r^2)^{1.5}(x^2 - y^2)^{1.5}$ average configuration[16,42] for which $\Delta E_v^e = 0$ and thus only influenced by the H_v^a term.

From eqs 4−7, the same E_{JT} value is obtained for $n(3z^2 - r^2) - n(x^2 - y^2) = 1$ and $Q_\theta^0 > 0$ (elongated geometry) as for $n(3z^2 - r^2) - n(x^2 - y^2) = -1$ and $Q_\theta^0 < 0$ (compressed geometry).[8,36] This equivalence is, however, destroyed when we consider tiny factors such as the anharmonicity in the e_g mode or the 3d−4s vibronic admixture.[16,42] The EPR spectra of d^9 ions in several cubic halides explored *up to now* show that the stable conformation corresponds to an elongated geometry.[7−10] However, the possible existence of true JT systems displaying a compressed geometry cannot be discarded at all despite the anharmonicity, if the complex is decoupled from the host lattice and the 3d−4s vibronic admixture both favor an elongated geometry.[16,29] Although it has been assumed[7,36,43,44] that the JT center formed in LiF:Ni^+ and NaF:Ni^+[43] displays a compressed geometry, there are serious arguments against the correctness of this assignment.[45,46] Subsequent EPR work carried out on NaCl:Ni^+,[47] $KMgF_3$:Ni^+,[48] or $CsCaF_3$:Ni^+[49] prove that the JT center exhibits an elongated geometry.

4. RESULTS AND DISCUSSION

4.1. Calculated Equilibrium Geometry for Pure K_2ZnF_4 and K_2MgF_4 Lattices. In a first step we have sought to check the reliability of the periodic calculations by comparing the calculated equilibrium geometry of pure K_2AF_4 (A = Zn, Mg) lattices with experimental results.[17,24] Values of lattice parameters a and c together with those corresponding to axial and equatorial A−F distances of host lattices, R_{ax}^H and R_{eq}^H, are collected in Table 1. As can be seen in that table, the deviation

Table 1. Values (in pm) of Lattice Parameters a and c Calculated in the Present Work for K_2BF_4 (B = Zn, Mg) Pure Lattices by Means of Periodic Calculations[a]

lattice	method	a	c	R_{eq}^H	R_{ax}^H	ref.
K_2ZnF_4	experimental	405.8	1310.9	202.9	202.6	17
	calculated	403.3	1298.4	201.7	202.9	
K_2MgF_4	experimental	398.0	1317.9	199.0	200.4	24
	calculated	394.5	1303.1	197.3	199.8	

[a]The values of axial and equatorial B−F distances are also given. All the calculated distances are compared with the corresponding experimental values.

of calculated values with respect to experimental ones does not exceed 1%. The calculations thus reproduce both R_{ax}^H and R_{eq}^H being close to R^H = 203 pm for K_2ZnF_4.

4.2. Calculated Equilibrium Geometry for Divalent Impurities in K_2ZnF_4 and K_2MgF_4. In a first step, we have explored the local equilibrium geometry in layered perovskites for impurities with a *closed shell* structure. The values of the equilibrium impurity-ligand distances, R_{ax}^0 and R_{eq}^0, for Cd^{2+} and Be^{2+} impurities calculated by means of periodic 56 atom supercells are gathered in Table 2. It can be noticed that although Cd^{2+} and Be^{2+} ions have a closed shell structure, the calculated R_{ax}^0 and R_{eq}^0 values are certainly different. In the case of K_2MgF_4:Cd^{2+}, the calculated values R_{ax}^0 = 223.1 pm and R_{eq}^0 = 211.9 pm point out that the CdF_6^{4-} unit is elongated along the crystal c axis. As shown in Table 2, such values are coincident with those derived through a calculation on a 37 atom cluster

Table 2. Equilibrium Values of Axial and Equatorial M−F Distances (in pm) Calculated for Closed Shell Impurities Cd^{2+} and Be^{2+} Doped in K_2ZnF_4 and K_2MgF_4 Lattices[a]

impurity	lattice	method	size	R_{eq}^0	R_{ax}^0
Cd^{2+}	K_2ZnF_4	periodic	56 ions	212.0	220.8
	K_2MgF_4	periodic	56 ions	211.9	223.1
	K_2MgF_4	cluster	37 ions	210.7	220.3
Be^{2+}	K_2ZnF_4	periodic	56 ions	191.1	168.4
	K_2MgF_4	periodic	56 ions	191.8	168.8
	K_2MgF_4	cluster	37 ions	185.4	171.8

[a]Results corresponding to periodic supercells and the B1WC hybrid functional are compared with those obtained by means of clusters and the GGA functional.

within 1.5%. These results confirm that, although the substitution of Mg^{2+} or Zn^{2+} by Cd^{2+} induces an outward ligand relaxation due to the higher size of the impurity with respect to the substituted host cation, the increase undergone by the axial distance, $R_{ax}^0 - R^H$ = 21 pm, is higher than $R_{eq}^0 - R^H$ = 10 pm. This fact simply reflects that the force constant for moving a ligand along the metal−ligand direction is higher for an equatorial ligand (K_{eq}) than for an axial ligand (K_{ax}) lying along the crystal c axis.[25] Values of the ratio $K_{eq}/K_{ax} \approx 2$ have been calculated for divalent impurities in these layered perovskites.[18] This significant difference between K_{eq} and K_{ax} can qualitatively be understood as equatorial F^- ligands are attached to divalent cations like Mg^{2+} or Zn^{2+} in the layer plane, while axial ligands are connected to *monovalent* K^+ ions (Figure 1). In other words, despite the fact that substitution of Mg^{2+} or Zn^{2+} by Cd^{2+} produces the *same* outward *force* on both axial and equatorial ligands, not all of them undergo the same displacement because the axial and equatorial force constants are *not equal*. This gives rise to a tetragonally elongated CdF_6 octahedron in the absence of any JT effect.

As the ionic radius of Be^{2+} is smaller than those of Mg^{2+} or Zn^{2+} ions, an *inward* ligand relaxation (Table 2) is found in K_2AF_4:Be^{2+} (A = Zn, Mg). Moreover, as $K_{eq} > K_{ax}$ then $R^H - R_{ax}^0 > R^H - R_{eq}^0$. This explains that the calculated local geometry around the Be^{2+} impurity corresponds to a D_{4h} compressed octahedron where the C_4 axis is again the crystal c axis.

In a second step, we have explored the equilibrium geometry of transition metal complexes with a ground state which is already an orbital singlet under O_h symmetry. The values of R_{ax}^0 and R_{eq}^0 derived from periodic supercell calculations for MnF_6^{4-} and NiF_6^{4-} complexes in K_2ZnF_4 and K_2MgF_4 lattices are gathered in Table 3. As the ionic radius of Mn^{2+} is higher than that of Mg^{2+} or Zn^{2+} ions, then values of $R_{ax}^0 - R^H$ and $R_{eq}^0 - R^H$ are found to be *both* positive, albeit $R_{ax}^0 - R^H > R_{eq}^0 - R^H$ again because $K_{eq} > K_{ax}$. Thus, the equilibrium geometry of the MnF_6^{4-} complex in such layered perovskites is found to correspond to an elongated octahedron along the crystal c axis.[18] This fact is thus in agreement with EPR data obtained on K_2AF_4:Mn^{2+} (A = Zn, Mg).[26,27] As shown in Table 3, the relaxation pattern derived through calculations on 37 atom clusters is close to that reached by means of periodic supercell calculations.

Bearing in mind that the ionic radius of Ni^{2+} is ∼10 pm smaller than that of Mn^{2+}, the $Zn^{2+} \rightarrow Ni^{2+}$ substitution in K_2ZnF_4 leads to tiny relaxation effects, where R_{ax}^0 and R_{eq}^0 are both around 200 pm as shown in Table 3.

Let us now discuss the equilibrium geometry obtained for Cu^{2+}-doped K_2ZnF_4 and K_2MgF_4 lattices by means of periodic

dx.doi.org/10.1021/ic400105z | Inorg. Chem. 2013, 52, 6923−6933

Table 3. Equilibrium Values of Axial and Equatorial M−F Distances Calculated for K_2ZnF_4:M^{2+} and K_2MgF_4:M^{2+} (M = Mn, Ni) Derived by Means of Periodic Calculations Using a Supercell of 56 Atoms[a]

impurity	lattice	method	R^0_{eq} (pm)	R^0_{ax} (pm)
Mn^{2+}	K_2ZnF_4	periodic	205.2	209.6
	K_2ZnF_4	cluster	203.9	208.0
	K_2MgF_4	periodic	205.3	212.1
	K_2MgF_4	cluster	202.5	208.2
Ni^{2+}	K_2ZnF_4	periodic	199.7	200.6
	K_2ZnF_4	cluster	199.0	199.2
	K_2MgF_4	periodic	199.9	202.1
	K_2MgF_4	cluster	198.1	200.2

[a]For comparison, R^0_{eq} and R^0_{ax} values calculated using a cluster of 37 atoms and the LDA functional are also given.

supercell calculations. To make sure that there is not an orthorhombic distortion in the {*a*, *b*} equatorial plane (Figure 1), such as is observed in the $CuCl_4(H_2O)_2^{2-}$ complex at low temperatures,[4,5,7,3] we have started the calculation assuming a local D_{2h} symmetry where two equatorial ligands in the trans position are at a distance R_{eq}^{s} from copper, while the two others are at a longer distance, R_{eq}^{l}. We have verified that all periodic calculations carried out for K_2ZnF_4:Cu^{2+} lead to a tetragonal equilibrium geometry where $R_{eq}^{s} = R_{eq}^{l}$ and the C_4 axis is just the crystal *c* axis. This result is fully consistent with all EPR and optical data.[12−14] In particular, EPR data prove that, in the 4−300 K temperature range, the local symmetry of K_2ZnF_4:Cu^{2+} is tetragonal and not orthorhombic while $g_\perp - g_0$ decreases *only* by 7%.[50] Values of the equilibrium distances, R^0_{ax} and R^0_{eq}, obtained for Cu^{2+}-doped K_2ZnF_4 and K_2MgF_4 are gathered in Table 4. It can be noticed that calculations on K_2ZnF_4:Cu^{2+}

Table 4. Equilibrium Values of Axial and Equatorial M−F Distances Calculated for Cu^{2+}-Doped K_2ZnF_4 and K_2MgF_4 Lattices Derived by Means of Periodic Calculations Using a Supercell of 56 Atoms[a]

lattice	method	size	R^0_{eq} (pm)	R^0_{ax} (pm)
K_2ZnF_4	periodic	56 ions	203.9	193.3
K_2ZnF_4	periodic	126 ions	204.1	193.1
K_2ZnF_4	cluster	69 ions	206.8	192.8
K_2MgF_4	periodic	56 ions	204.1	194.5
K_2MgF_4	cluster	37 ions	204.7	192.1

[a]For comparison, the R^0_{eq} and R^0_{ax} values calculated using a cluster of 37 atoms and the LDA functional are also given.

using 56 and 126 atom supercells both lead to a slightly compressed CuF_6^{4-} complex along the crystal *c* axis where the unpaired electron is in the antibonding $a_{1g}^*(\sim 3z^2 - r^2)$ orbital ($^2A_{1g}$ ground electronic state) and $R^0_{eq} - R^0_{ax} = 11$ pm. This figure is then about three times smaller than $R^0_{eq} - R^0_{ax} = 29$ pm estimated through the *parametrized* JT model.[15,50] In the case of K_2MgF_4:Cu^{2+}, the periodic calculation gives a value of $R^0_{eq} - R^0_{ax} = 9.6$ pm which is slightly smaller than that obtained for K_2ZnF_4:Cu^{2+}. For K_2MgF_4:Cu^{2+}, as shown in Table 4, periodic and cluster calculations provide similar patterns.

It is worth noting that only one energy minimum, and not three equivalent such as happens in a JT system, is found in our calculations. This is consistent with the fact that absorption spectra collected with the electric field of the light polarized either parallel or perpendicular to the crystal *c* axis are *different*.[13]

Bearing in mind that Cu^{2+} and Ni^{2+} ions have a close ionic radius, it is interesting to compare the results found for K_2ZnF_4:Cu^{2+} (Table 4) with those for K_2ZnF_4:Ni^{2+} (Table 3). In the latter case, the $Zn^{2+} \rightarrow Ni^{2+}$ substitution gives rise to a small inward relaxation where R^0_{ax} and R^0_{eq} are both practically equal to 200 pm (Table 3) and thus a bit smaller than $R^H = 203$ pm. By contrast, for K_2ZnF_4:Cu^{2+} all calculations collected in Table 4 give $R^H - R^0_{ax} \gg R^0_{eq} - R^H$, pointing out that in this case there is *an additional mechanism* responsible for the equilibrium geometry. For gaining a better insight into the origin of this fact, a detailed analysis of the electronic structure is now necessary.

4.3. Calculated Electronic States and Optical Spectrum for K_2ZnF_4:Cu^{2+}. Once the equilibrium geometry and the nature of the electronic ground state for K_2ZnF_4:Cu^{2+} have been well established, it is crucial to explore the energy of the so-called d−d excitations involving a hole transfer from $a_{1g}^*(\sim 3z^2 - r^2)$ to $b_{1g}^*(\sim x^2 - y^2)$, $b_{2g}^*(xy)$, and $e_g^*(xz;yz)$ orbitals (Figure 2). Accordingly, particular attention has been paid to calculate the energy difference between the excited $^2B_{1g}$, $^2B_{2g}$, and ^2E_g states and the ground state $^2A_{1g}$ not only at the final equilibrium geometry ($R^0_{eq} = 204$ pm, $R^0_{ax} = 193$ pm) but especially at the *initial* one where the Cu^{2+} impurity enters the Zn^{2+} site in K_2ZnF_4 and $R_{eq} = R_{ax} = R^H = 203$ pm. Results on K_2ZnF_4:Cu^{2+} are displayed in Figure 3. Very similar findings have been obtained for K_2MgF_4:Cu^{2+}.

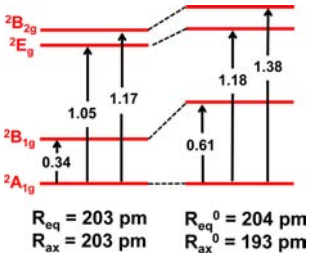

Figure 3. Pictorial description of the DFT calculated values of the energies (in eV) corresponding to the electronic transitions from the ground state $^2A_{1g}$ of K_2MgF_4:Cu^{2+} to the excited states $^2B_{1g}$, ^2E_g, and $^2B_{2g}$, at the optimized equilibrium geometry of the ground state, R^0_{eq} = 204 pm and R^0_{ax}= 193 pm (right) and at the *initial* one where Cu^{2+} impurity enters the Zn^{2+} site in K_2ZnF_4 and $R_{eq} = R_{ax} = 203$ pm (left).

Experimental optical absorption data on K_2ZnF_4:Cu^{2+} crystals have been measured in the 0.90−1.60 eV range by Riley et al.[13,14,51] A broad band peaked at 1.3 eV has been assigned to the $^2A_{1g} \rightarrow {}^2E_g$ transition. The calculated value of 1.2 eV for that transition in Figure 3 at the equilibrium geometry ($R^0_{eq} = 204$ pm, $R^0_{ax} = 193$ pm) is thus close to the experimental value. Moreover, Riley et al. point out that as the employed samples are *too dilute* in Cu^{2+} impurities, a very weak broad band, whose maximum is about 0.70 eV, is also observed in the optical spectra of K_2ZnF_4:Cu^{2+}.[13] The origin of such a broad band is ascribed by Riley et al. to the $^2A_{1g} \rightarrow {}^2B_{1g}$ transition. According to the present calculations, such a transition is found to be at 0.61 eV (Figure 3) at the equilibrium geometry of the ground state, and thus there is reasonable agreement with the experimental figure. The $^2A_{1g} \rightarrow {}^2B_{2g}$ transition energy is calculated to be equal to 1.38 eV, while it is placed at 1.33 eV according to experimental data.[13,51]

dx.doi.org/10.1021/ic400105z | *Inorg. Chem.* 2013, 52, 6923−6933

Seeking to understand why the $^2A_{1g} \rightarrow {}^2B_{1g}$ transition is broad, we have also calculated the energy of the $^2B_{1g}$ excited state at its equilibrium geometry using a cluster of 69 ions. It turns out that at the equilibrium geometry (described by R^0_{eq} = 199 pm and R^0_{ax} = 214 pm), the $^2B_{1g}$ state is laying only 0.24 eV above the ground state. This means that, while the maximum of the band associated with the $^2A_{1g} \rightarrow {}^2B_{1g}$ transition is found at ~0.7 eV, the corresponding zero-phonon line would be only at ~0.3 eV. This big difference is thus consistent with the observation of a very broad band arising from such a transition.[13]

Let us now explore whether the experimental energy for the $^2A_{1g} \rightarrow {}^2B_{1g}$ transition, $E(^2A_{1g} \rightarrow {}^2B_{1g})$, in K_2ZnF_4:Cu^{2+} can or cannot be explained *assuming* that the gap between $^2A_{1g}$ and $^2B_{1g}$ states is the result of a JT distortion. According to eq 4

$$E(^2A_{1g} \rightarrow {}^2B_{1g}) = -2V_{1e}Q^0_\theta;\ Q^0_\theta = (2/\sqrt{3})\{R^0_{ax} - R^0_{eq}\} \quad (8)$$

The value of the linear coupling coefficient, V_{1e}, calculated for Cu^{2+}-doped cubic oxides is found to be in the range 0.5−1.1 eV/Å.[52] Furthermore, we have calculated V_{1e} = 1.1 eV/Å for $KZnF_3$:Cu^{2+} where there is a static JT effect[10,14] because this perovskite is perfectly cubic. Using this V_{1e} value and $E(^2A_{1g} \rightarrow {}^2B_{1g})$ = 0.7 eV measured for K_2ZnF_4:Cu^{2+}, we get $R^0_{ax} - R^0_{eq}$ = 33 pm, which is close to that proposed in ref 15. Nevertheless, this figure is *three times* higher than the $R^0_{ax} - R^0_{eq}$ = 11 pm obtained from the present periodic supercell calculations for K_2ZnF_4:Cu^{2+} (Table 4). Thus, in view of this serious discrepancy, it is hard to invoke the JT effect as responsible for the equilibrium geometry in K_2ZnF_4:Cu^{2+}. Moreover, this analysis reveals that the 0.70 eV gap between $^2A_{1g}$ and $^2B_{1g}$ states observed experimentally for K_2ZnF_4:Cu^{2+} can hardly be understood only through the *small* distortion ($R^0_{ax} - R^0_{eq}$ = 11 pm) calculated for the CuF_6^{4-} complex in K_2ZnF_4. This conclusion is also supported by results on the JT center formed in NaCl:Rh^{2+}[53] where $E(^2A_{1g} \rightarrow {}^2B_{1g})$ = 0.70 eV when $R^0_{ax} - R^0_{eq}$ = 26 pm.[54]

Seeking to shed light on this surprising situation, we have looked in detail into the dependence of the calculated energy $E(^2A_{1g} \rightarrow {}^2B_{1g})$ on equatorial and axial Cu^{2+}−F^- distances. As a salient feature, it is found that when $R_{eq} = R_{ax}$, the a_{1g}*($\sim 3z^2 - r^2$) and b_{1g}*($\sim x^2 - y^2$) levels of K_2ZnF_4:Cu^{2+} are *not degenerate*. Indeed, as is shown in Figure 3, the value of the $^2A_{1g} \rightarrow {}^2B_{1g}$ excitation is calculated to be equal to 0.34 eV when $R_{eq} = R_{ax}$ = 203 pm. In the same vein, the b_{2g}*($\sim xy$) and e_g*($xz;yz$) levels are found to be nondegenerate when $R_{eq} = R_{ax}$. In fact, according to Figure 3, the $^2B_{2g}$ state is lying 0.12 eV above ^2E_g when the axial and equatorial distances are strictly equal.

The present findings thus confirm that the energy difference between $^2A_{1g}$ and $^2B_{1g}$ states observed experimentally does *not only* reflect that $R^0_{ax} \neq R^0_{eq}$. Indeed about 50% of the $^2A_{1g} \rightarrow {}^2B_{1g}$ excitation energy in K_2ZnF_4:Cu^{2+} is *already* present when the fluorine octahedron is not distorted. The existence of a gap between $^2A_{1g}$ and $^2B_{1g}$ states, and also between ^2E_g and $^2B_{2g}$ states, when $R_{eq} = R_{ax}$ stresses that the actual symmetry felt by the active electrons confined in the CuF_6^{4-} complex is not cubic but tetragonal. This conclusion is *in principle* puzzling because the two gaps should be zero when $R_{eq} = R_{ax}$ provided the CuF_6^{4-} complex is *truly isolated*.

Nevertheless, complexes formed in *insulating materials* are never isolated but embedded in a lattice formed by *charged* ions. Therefore, although active electrons coming from a transition metal impurity like Cu^{2+} in K_2ZnF_4 are *localized* in the CuF_6^{4-} complex, they are *also* feeling the electrostatic potential, $V_R(\mathbf{r})$, due to the rest of the lattice ions. The form of $V_R(\mathbf{r})$ potential for CuF_6^{4-} in K_2ZnF_4 when $\mathbf{r}$ is running along *a* and *c* axes is shown in Figure 4 and reflects the *tetragonal*

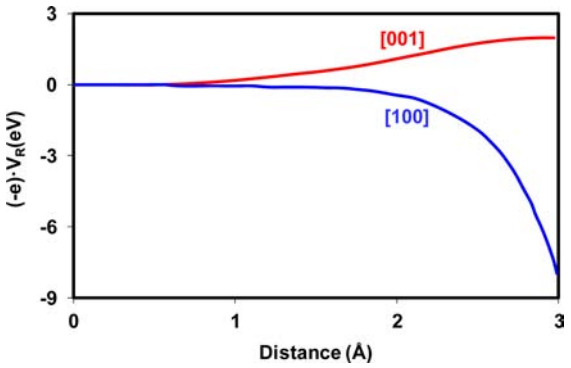

Figure 4. Electrostatic potential, $V_R(\mathbf{r})$, produced on a seven atom CuF_6^{4-} complex by the rest of ions of the K_2ZnF_4 lattice. Potential is depicted along [100] and [001] crystalline directions.

symmetry of K_2AF_4 (A = Zn, Mg) host lattices.[25] It can be noticed that this electrostatic potential, $V_R(\mathbf{r})$, tends to increase the energy of the a_{1g}*($\sim 3z^2 - r^2$) orbital and to decrease that of the b_{1g}*($\sim x^2 - y^2$) one. Therefore, the results of Figure 4 explain qualitatively the existence of a gap between $^2A_{1g}$ and $^2B_{1g}$ states even when $R_{eq} = R_{ax}$. Such a gap directly comes from the internal electric field, $\mathbf{E}_R(\mathbf{r}) = -\nabla V_R(\mathbf{r})$, displaying tetragonal symmetry, to which the CuF_6^{4-} unit in K_2ZnF_4 is inevitably subject. In other words, for explaining the properties of Cu^{2+}-doped K_2ZnF_4, we need to consider *both* the CuF_6^{4-} unit and the internal electric field $\mathbf{E}_R(\mathbf{r})$, and thus the *global* symmetry is tetragonal even though all the Cu^{2+}−F^- distances are equal.

It is worth noting that due to the D_{4h} symmetry of the crystal, there is no internal electric field, $\mathbf{E}_R(\mathbf{r})$, when active electrons, confined in the CuF_6^{4-} unit, are on the impurity, placed at $\mathbf{r}$ = 0 (Figure 4). However, this statement is no longer true when we consider that antibonding electrons *also* spend some time around the ligands where the value of the internal electric field, $\mathbf{E}_R(\mathbf{r})$, is certainly nonzero (Figure 4).

The role played by the internal electric field has usually been ignored when seeking to understand the origin of optical and magnetic properties due to transition metal complexes in insulators. However, it has been shown that $\mathbf{E}_R(\mathbf{r})$ is mainly responsible for the different colors of gemstones like ruby, emerald, or alexandrite.[55,56] In the same vein, the internal electric field, which is more intense in the inverse perovskite $LiBaF_3$ than in a normal perovskite like $KMgF_3$, has been shown to be the origin of the distinct optical and EPR spectra displayed by Mn^{2+}, Co^{2+}, Ni^{2+}, and Cr^{3+} impurities in such lattices.[57]

4.4. Origin of the Ligand Distortion in K_2ZnF_4:Cu^{2+}. According to the analysis carried out in the preceding section, there is no orbital degeneracy when $R_{eq} = R_{ax}$, which is the most distinctive characteristic of a JT effect. Furthermore, there is *no symmetry change* on going from the initial situation ($R_{eq} = R_{ax}$ = 203 pm) to the equilibrium geometry (R^0_{eq} = 204 pm, R^0_{ax} = 193 pm) in K_2ZnF_4:Cu^{2+} and no other distortions typical of JT systems (elongation or compression along *a* or *b* axes) appear, even metastable ones. In both situations, the global symmetry,

dx.doi.org/10.1021/ic400105z | Inorg. Chem. 2013, 52, 6923−6933

corresponding to the CuF_6^{4-} complex *under* the electrostatic potential, $V_R(\mathbf{r})$, is always tetragonal. Therefore, the ligand relaxation taking place in $K_2ZnF_4:Cu^{2+}$ cannot properly be ascribed to a static JT effect which necessarily gives rise to symmetry breaking and different possible orientations of the system.[7,8,40] Reasoning in a similar way the tetragonal distortion cannot be attributed to the pseudo-Jahn−Teller coupling between A_{1g} and B_{1g} states. Indeed the pseudo-Jahn−Teller effect is usually related to the existence of symmetry breaking in an electronic ground state with no orbital degeneracy.

The distortion associated with the equilibrium geometry of $K_2ZnF_4:Cu^{2+}$ involves the activation of *two different* a_{1g} modes which appear in a complex with D_{4h} symmetry, and thus the tetragonal symmetry is always conserved. In short, such modes are a linear combination of a_{1g}^{ax} and a_{1g}^{eq} modes corresponding to the symmetric displacements of two axial and four equatorial ligands, respectively (Figure 5). In our calculations, we have

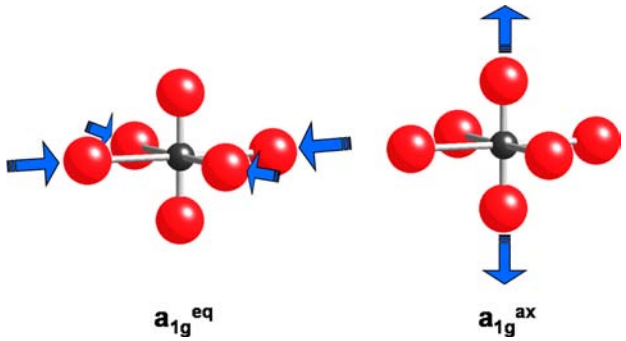

Figure 5. Equatorial, a_{1g}^{eq}, and axial, a_{1g}^{ax}, a_{1g} modes in the CuF_6^{4-} complex with D_{4h} symmetry.

found that one of such modes is described by $0.155a_{1g}^{eq} + 0.988a_{1g}^{ax}$, pointing out that it has a definite axial character. We have seen in section 4.2 that the substitution of Zn^{2+} by impurities like Mn^{2+} or Ni^{2+} produces a ligand relaxation where $R_{ax}^0 - R^H$ and $R_{eq}^0 - R^H$ have the same sign but $|R_{ax}^0 - R^H| > |R_{eq}^0 - R^H|$. This has been shown to arise from the different ionic radius of Zn^{2+} and the impurity and the elastic anisotropy of the host lattice[18] making $K_{eq} > K_{ax}$.

For understanding the origin of the ligand relaxation in $K_2ZnF_4:Cu^{2+}$, it is useful to determine first the equilibrium R_{ax}^* and R_{eq}^* values corresponding to the $(3z^2 - r^2)^{1.5}(x^2 - y^2)^{1.5}$ average configuration. In this configuration, the *same number* of electrons is placed on two orbitals, a situation which is thus similar to the ground state of a Ni^{2+} impurity. Calculations carried out on a cluster of 69 ions give $R_{eq}^* = 203.1$ pm and $R_{ax}^* = 202.6$ pm. This result supports that the ligand relaxation due only to size effects is negligible in $K_2ZnF_4:Cu^{2+}$, a fact consistent with the closeness of ionic radii of $Zn^{2+}$and Cu^{2+}.

Let us now consider the actual configuration, $(x^2 - y^2)^2(3z^2 - r^2)^1$, corresponding to the ground state of $K_2ZnF_4:Cu^{2+}$. If we call $\rho(\mathbf{r};x^2 - y^2)$ and $\rho(\mathbf{r};3z^2 - r^2)$, the electronic densities associated with $b_{1g}^*(\sim x^2 - y^2)$ and $a_{1g}^*(\sim 3z^2 - r^2)$ orbitals, respectively, both belong to the A_{1g} symmetry of the D_{4h} group. This situation is thus different from that found under strict O_h symmetry where the two orbitals are degenerate and only the quantity $\rho(\mathbf{r};x^2 - y^2) + \rho(\mathbf{r};3z^2 - r^2)$ belongs to the A_{1g} representation of the cubic group. This means that there is some relation between $\rho(\mathbf{r};x^2 - y^2)$ and $\rho(\mathbf{r};3z^2 - r^2)$ in O_h symmetry which is responsible for the validity of the center-of-gravity theorem. Nevertheless, $\rho(\mathbf{r};x^2 - y^2)$ and $\rho(\mathbf{r};3z^2 - r^2)$ are independent under the tetragonal symmetry present in $K_2ZnF_4:Cu^{2+}$. Despite this fact, as in $K_2ZnF_4:Cu^{2+}$, the $b_{1g}^*(\sim x^2 - y^2)$ orbital has an equatorial character while $a_{1g}^*(\sim 3z^2 - r^2)$ is mainly axial; there is an imbalance of the electronic charge in the two regions because the former is fully populated and the latter only half populated. In other words, on passing from the equilibrium situation for the $(3z^2 - r^2)^{1.5}(x^2 - y^2)^{1.5}$ configuration ($R_{eq}^* = R_{ax}^* = R^* = 203$ pm) to the final equilibrium geometry (Table 4) associated with the actual configuration, $(x^2 - y^2)^2(3z^2 - r^2)^1$, there is a change of electronic density, $\Delta\rho(\mathbf{r})$, given by

$$\Delta\rho(\mathbf{r}) = -(1/2)\rho(\mathbf{r};\, 3z^2 - r^2) + (1/2)\rho(\mathbf{r};\, x^2 - y^2) \tag{9}$$

Therefore, in this step there is an increase of electronic charge in the equatorial plane, while there is a reduction in the axial region. This explains albeit qualitatively that $\Delta\rho(\mathbf{r})$ favors that $R_{eq}^0 > R^*$ while, on the contrary, $R_{ax}^0 < R^*$. Moreover, as $K_{eq}/K_{ax} \approx 2$,[18,25] the value $|R^* - R_{ax}^0|$ is found to be much higher than $|R^* - R_{eq}^0|$. According to the results in Table 4, $R_{eq}^0 - R^*$ is lying between 1 and 3.5 pm, while $R^* - R_{ax}^0$ is practically equal to 10 pm. Therefore, the ratio $(R^* - R_{ax}^0)/(R_{eq}^0 - R^*)$ is found to be certainly higher than 2, and thus eq 2, characteristic of a static JT effect, is not fulfilled.

It should be remarked that in a true JT system the $(x^2 - y^2)^2(3z^2 - r^2)^1$ and $(3z^2 - r^2)^2(x^2 - y^2)^1$ configurations have the same energy when the octahedron is undistorted.[8,36] For this reason, if we compare a hole in $3z^2 - r^2$ and $Q_\theta < 0$ with a hole in $x^2 - y^2$ and $Q_\theta > 0$, the energy difference between these configurations is below 0.015 eV for Cu^{2+} and Ag^{2+} impurities in cubic oxides, as it is due to tiny effects such as the anharmonicity in the e_g mode.[39,40,52] By contrast, for $K_2ZnF_4:Cu^{2+}$, the two $(x^2 - y^2)^2(3z^2 - r^2)^1$ and $(3z^2 - r^2)^2(x^2 - y^2)^1$ configurations are no longer equivalent when $R_{eq} = R_{ax} = 203$ pm, as there is a gap of 0.34 eV between them, and the HOMO orbital is $a_{1g}^*(\sim 3z^2 - r^2)$. Thus, as it has been pointed out, the only way of reducing the energy of the ground state configuration in $K_2ZnF_4:Cu^{2+}$ is through a distortion making $R_{eq}^0 > R^*$ and $R_{ax}^0 < R^*$.

While the previous paragraphs could indicate that the distortion in $K_2ZnF_4:Cu^{2+}$ is somewhat similar to a JT effect, we would like to highlight here that a crucial point in this analysis concerns the energy shift undergone by $b_{1g}^*(\sim x^2 - y^2)$ and $a_{1g}^*(\sim 3z^2 - r^2)$ orbitals on passing from $R_{eq} = R_{ax} = 203$ pm to the equilibrium geometry ($R_{eq}^0 = 204$ pm, $R_{ax}^0 = 193$ pm). The main results are depicted in Figure 6. It can be noticed that

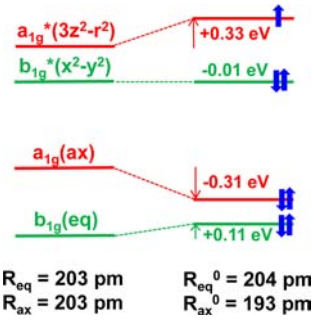

Figure 6. Qualitative description of the energy shift of antibonding $b_{1g}^*(\sim x^2 - y^2)$ and $a_{1g}^*(\sim 3z^2 - r^2)$ and bonding $a_{1g}(ax)$, and $b_{1g}(eq)$ orbitals of a CuF_6^{4+} complex in K_2ZnF_4 on going from $R_{eq} = R_{ax} = 203$ pm to the equilibrium geometry, $R_{eq}^0 = 204$ pm, $R_{ax}^0 = 193$ pm.

dx.doi.org/10.1021/ic400105z | Inorg. Chem. 2013, 52, 6923−6933

in that process, where axial ligands are approaching the Cu^{2+} ion, the energy of the $a_{1g}^*(\sim 3z^2 - r^2)$ orbital increases by a quantity $\delta\varepsilon(3z^2 - r^2) = 0.33$ eV. This increase is, however, not compensated by the corresponding energy variation of the $b_{1g}^*(\sim x^2 - y^2)$ orbital, because $\delta\varepsilon(x^2 - y^2) = -0.01$ eV. Therefore, these results stress that for K_2ZnF_4:Cu^{2+}, the quantity $2\delta\varepsilon(x^2 - y^2) + \delta\varepsilon(3z^2 - r^2)$ is *positive* and not negative, as it happens in a JT effect. This means that the stabilization process in K_2ZnF_4:Cu^{2+} cannot be understood considering *only* the energy shift and the different population of two $b_{1g}^*(\sim x^2 - y^2)$ and $a_{1g}^*(\sim 3z^2 - r^2)$ antibonding orbitals such as occurs in the JT effect (eq 7). We have verified that bonding orbitals with an axial character play a relevant role in the stabilization mechanism. This can be seen in Table 5 where the changes undergone by the most relevant orbitals of the perfect octahedron are shown in two steps: (1) adding the effect of the external electric field $V_R(\mathbf{r})$ but maintaining the octahedral geometry and (2) considering the tetragonal distortion. The most dramatic changes correspond to step 1, involving large electron transfers (20−25%) toward the axial fluorine ions (F_{ax}) in orbitals $a_{1g}^*(\sim 3z^2 - r^2)$ and a_{1g}(ax). It can be appreciated in Table 5 that a large part of this charge comes from a_{1g}(eq) orbitals. This is accompanied by a similar transfer of 3d(Cu) character between a_{1g}(eq) and a_{1g}(ax) bonding orbitals. Compared with these changes, those occurring along the tetragonal distortion of step 2 (third column in Table 5) are certainly more modest.

Table 5. Orbital Energies, ε (in eV), and Mulliken Population Analysis (in %) on a_{1g} and b_{1g} Orbitals with Antibonding (Marked with an Asterisk) and Equatorial (eq Superindex) and Axial (ax Superindex) Bonding Character Calculated for the Ground State of the CuF_6^{4-} Complex in Three Different Situations: (a) Purely Isolated Complex with Octahedral Symmetry and $R_{eq} = R_{ax} = 203$ pm; (b) the CuF_6^{4-} Complex Feels the Electrostatic Potential $V_R(\mathbf{r})$ from the K_2ZnF_4 Host Lattice but There Is No Distortion ($R_{eq} = R_{ax} = 203$ pm); (c) the CuF_6^{4-} Complex Feels $V_R(\mathbf{r})$ and Is at the Equilibrium Geometry Found for K_2ZnF_4:Cu^{2+} ($R_{eq}^0 = 204$ pm, $R_{ax}^0 = 193$ pm)[a]

orbital		isolated undistorted complex	undistorted complex under $V_R(\mathbf{r})$	distorted complex under $V_R(\mathbf{r})$
	E	−15.62	−98.61	−98.75
a_{1g}^*	ε	14.52	−5.77	−5.35
	4s	0.1	0.4	0.4
	3d($3z^2 - r^2$)	72.2	70.1	70.0
	2p(F_{eq})	14.9	7.4	7.6
	2p(F_{ax})	8.7	20.7	19.1
b_{1g}^*	ε	13.71	−6.99	−6.85
	3d($x^2 - y^2$)	66.6	74.1	75.2
	2p(F_{eq})	29.5	23.9	22.8
	2p(F_{ax})	3.5	1.5	1.5
b_{1g}	ε	9.42	−11.58	−11.42
	3d($x^2 - y^2$)	33.7	25.5	24.5
	2p(F_{eq})	64.1	73.3	74.3
a_{1g}(eq)	ε	9.30	−12.05	−11.94
	4s	0.3	1.9	1.9
	3d($3z^2 - r^2$)	24.7	2.5	0.5
	2p(F_{eq})	52.1	89.3	84.2
	2p(F_{ax})	19.7	6.1	12.6
a_{1g}(ax)	ε	8.72	−10.81	−11.07
	4s	7.8	1.4	1.4
	3d($3z^2 - r^2$)	2.9	27.5	28.3
	2p(F_{eq})	30.9	2.7	8.0
	2p(F_{ax})	57.9	67.0	61.5

[a]Total energies, E (in eV), are also given.

As is shown in Figure 6, the energy of the bonding a_{1g}(ax) orbital, with a dominant F_{ax} character, is the only one that decreases (−0.31 eV) on going from $R_{eq} = R_{ax} = 203$ pm to the equilibrium geometry. This negative energy shift is strong enough to compensate all the positive energy shifts occurring in orbitals like $a_{1g}^*(\sim 3z^2 - r^2)$ and $b_{1g}^*(\sim x^2 - y^2)$ and leads to an overall stabilization of the distortion. While this stabilization associated to the change of covalency has been associated to the pseudo-Jahn−Teller effect, the authors consider (at difference with the general definition given in ref 8) that this denotation is better reserved for problems where a symmetry-breaking distortion produces the electronic state mixing.

5. FINAL REMARKS

The analysis carried out in this work proves that the ligand relaxation in K_2ZnF_4:Cu^{2+} cannot be understood in terms of a static JT effect such as happens for $CsCdF_3$:Cu^{2+} or $KZnF_3$:Cu^{2+}.[9,10,14] First of all, there is no symmetry breaking on passing from the initial situation (characterized by $R_{eq} = R_{ax} = 203$ pm) to the equilibrium geometry, nor are there several accessible minima as occurs in a true JT effect. Indeed, from the beginning, the CuF_6^{4-} complex has been shown to be subject to the action of the internal electric field, displaying tetragonal symmetry, produced by the rest of the ions of the K_2ZnF_4 lattice. Moreover, periodic supercell calculations point out that equilibrium geometry involves only a slight distortion ($R_{eq}^0 = 204$ pm, $R_{ax}^0 = 193$ pm) clearly dominated by the motion of axial ligands which in turn arises from the difference between the equatorial and axial force constants, with $K_{eq}/K_{ax} \approx 2$,[18,25] thus stressing again the tetragonal character of the host lattice. As a salient feature, it has been shown that the stabilization energy associated with the distortion in K_2ZnF_4:Cu^{2+} does not come from the antibonding $b_{1g}^*(\sim x^2 - y^2)$ and $a_{1g}^*(\sim 3z^2 - r^2)$ orbitals, such as happens when the JT effect takes place. In fact, in K_2ZnF_4:Cu^{2+}, the orbital energy coming from the three antibonding electrons placed in $b_{1g}^*(\sim x^2 - y^2)$ and $a_{1g}^*(\sim 3z^2 - r^2)$ orbitals increases along the relaxation process, and thus the required energy gain involves fully occupied bonding orbitals, as is usually found in the realm of chemical bonding.

From the present analysis, the compressed geometry exhibited by CuF_6^{4-} in K_2ZnF_4:Cu^{2+} is greatly due to the internal electric field felt by the complex. At the same time, the existence of that internal field makes it possible to conciliate the *small* $R_{eq}^0 - R_{ax}^0 = 11$ pm value derived from the calculations with the large gap (0.7 eV) between $^2A_{1g}$ and $^2B_{1g}$ states measured experimentally.[13] Indeed, the internal field with tetragonal symmetry breaks the degeneracy of $a_{1g}^*(\sim 3z^2 - r^2)$ and $b_{1g}^*(\sim x^2 - y^2)$ orbitals when the fluorine octahedron is undistorted, thus the *only* way of obtaining an *additional* gain of electronic energy in the $(\sim x^2 - y^2)^2(\sim 3z^2 - r^2)^1$ configuration is through the compression of the CuF_6^{4-} octahedron. Moreover, the splitting between $a_{1g}^*(\sim 3z^2 - r^2)$ and $b_{1g}^*(\sim x^2 - y^2)$ orbitals when $R_{eq} = R_{ax} = 203$ pm accounts

dx.doi.org/10.1021/ic400105z | Inorg. Chem. 2013, 52, 6923−6933

for about half the experimental gap between $^2A_{1g}$ and $^2B_{1g}$ states in $K_2ZnF_4:Cu^{2+}$.

It should be noticed now that there is another remarkable difference between $K_2ZnF_4:Cu^{2+}$ and systems like $CsCdF_3:Cu^{2+}$ or $KZnF_3:Cu^{2+}$ displaying a static JT effect.[9,10,14] In fact, though in the last cases the CuF_6^{4-} complex is also subject to an internal field, it has a cubic symmetry, and then it does not give rise to any splitting between $a_{1g}^*(\sim 3z^2 - r^2)$ and $b_{1g}^*(\sim x^2 - y^2)$ orbitals when $R_{eq} = R_{ax}$. It should be noted that while $E(^2A_{1g} \rightarrow {}^2B_{1g}) = 0.70$ eV for $K_2ZnF_4:Cu^{2+}$, the separation between A_{1g} and B_{1g} states for $KZnF_3:Cu^{2+}$ should be *smaller than* 0.5 eV for the JT system $KZnF_3:Cu^{2+}$ according to the experimental data by Dubicki et al.[14] Supporting this view, calculations carried out on $KZnF_3:Cu^{2+}$ give $E(^2B_{2g} \rightarrow {}^2A_{1g}) = 0.39$ eV at the ground state equilibrium geometry ($R_{ax}^0 = 210$ pm, $R_{eq}^0 = 197$ pm).

Although the role of the internal field $\mathbf{E}_R(\mathbf{r})$ for explaining the properties of transition metal complexes in insulators has often been ignored, it is at the origin of several relevant properties. For instance, it accounts for the color shift in gemstones like ruby, emerald, or alexandrite.[55,56] On the other hand, the existence of $\mathbf{E}_R(\mathbf{r})$ explains a puzzling fact observed[58] for the unperturbed CrF_6^{3-} complex formed in $K_2MgF_4:Cr^{3+}$. Indeed the corresponding EPR spectra exhibit a clear *tetragonal* symmetry despite *ab initio* calculations proving that the complex is perfectly octahedral with $R_{eq} = R_{ax} = 189$ pm.[59]

According to the analysis carried out in section 4.4, the driving force behind the distortion in $K_2ZnF_4:Cu^{2+}$ is the differential density $\Delta\rho(\mathbf{r}) = -(1/2)\rho(\mathbf{r};3z^2 - r^2) + (1/2)\rho(\mathbf{r};x^2 - y^2)$. Although a seemingly similar situation holds for a d^9 ion under strict cubic symmetry in this case $\rho(\mathbf{r};3z^2 - r^2) + \rho(\mathbf{r};x^2 - y^2)$ is a cubic invariant, a fact which is behind the validity of the center-of-gravity theorem.[29] By contrast, this is no longer true for $K_2ZnF_4:Cu^{2+}$ where there is not any relation between $\rho(\mathbf{r};3z^2 - r^2)$ and $\rho(\mathbf{r};x^2 - y^2)$ due to the symmetry lowering. Moreover, in a static JT effect, the driving force can be $\Delta\rho(\mathbf{r})$ or $-\Delta\rho(\mathbf{r})$ as the two $(x^2 - y^2)^2(3z^2 - r^2)^1$ and $(x^2 - y^2)^1(3z^2 - r^2)^2$ configurations are in principle equivalent, while this is not the case for $K_2ZnF_4:Cu^{2+}$. In this case, the experimental $g_\perp - g_0$ value decreases only by 7% on passing from $T = 4$ K ($g_\perp = 2.386$)[12,50] to $T = 300$ K, a fact which is hardly compatible with a static JT effect. Indeed in systems displaying a static JT effect at low temperatures, an average isotropic EPR spectrum is *already* observed at $T = 160$ K[60] even for barriers as high as 0.13 eV.[61]

It is important to note here that, while Ham[36] has shown that a static JT effect cannot be observed without a strain that lowers the high symmetry conformation of the system, this argument cannot be extrapolated to systems whose intrinsic structure displays low symmetry. The main reason is that while in the first case the nature of the strain is *random*, meaning that the probability for a particular center to be oriented in the *x*, *y*, or *z* directions is exactly the same, for K_2ZnF_4 all Cu^{2+} centers will inevitably be oriented along the tetragonal *c* axis of the crystal.

Very often the distortions associated with d^9 ions in insulating lattices have been attributed to the JT effect.[62] The present study on $K_2ZnF_4:Cu^{2+}$ underlines that such an assumption can be wrong, especially when dealing with host lattices which are not cubic. On one hand, we have shown that, using closed-shell dopants, strong tetragonal distortions around the impurity site are not necessarily connected with degenerate levels, while, on the other hand, the main source of stabilization energy along the distortion mode of $K_2ZnF_4:Cu^{2+}$ is due to deep bonding orbitals. Even more, the presence of a d^9 ion in a cubic site does *not necessarily* mean that a JT is going to take place. Supporting this view, the equilibrium geometry of the Cu^{2+}-doped cubic SrF_2[63] or $SrCl_2$[7] lattices is not the result of a static JT effect, with a ligand distortion described by an even mode but corresponds to an off-center motion of the Cu^{2+} ion along ⟨100⟩ directions driven by an odd t_{1u} mode.[64,29]

The present results underline the usefulness of *ab initio* calculations for unveiling the actual origin of the equilibrium geometry and optical properties of Cu^{2+} impurities in a layered compound like K_2ZnF_4. The complexity and subtleties involved in a seemingly simple case like $K_2ZnF_4:Cu^{2+}$ are thus missed when a parametrized JT model is used where the key role played by the internal electric field is not taken into consideration. In fact, our calculations show that these models cannot be applied without careful consideration because while direct fitting may reproduce the experimental data, the parameters obtained in this manner lack chemical meaning. Accordingly, the present study on the model system $K_2ZnF_4:Cu^{2+}$ can be useful for better understanding the properties of d^9 and also d^4 and d^7 ions in *other* layered compounds.

It has been shown that the equilibrium geometry of divalent impurities in K_2AF_4 (A = Zn, Mg) lattices obtained by means of finite clusters are certainly close to those obtained through periodic supercell calculations. This coincidence is quite reasonable because electrons in good insulating materials are *localized*, a point which has been emphasized by Kohn.[65,66] For this reason, a cluster containing the complex (when active electrons are localized) and a buffer together with the internal field due to rest of the ions outside the cluster usually suffices for reproducing the main properties associated with an impurity in an insulating lattice.

It is worth noting that calculations have also been carried out on $K_2MgF_4:Ni^+$ where EPR data prove[67] that the unpaired electron is placed in the $b_{1g}^*(\sim x^2 - y^2)$ orbital. This fact is confirmed by both periodic and cluster calculations leading to an elongated equilibrium geometry where $R_{ax}^0 - R_{eq}^0$ is found to be ∼10 pm. As was earlier pointed out,[25] this surprising result arises from the small 3d−4s separation in a free Ni^+ ion (∼2 eV). In fact, as under the tetragonal internal field, the $3d(3z^2 - r^2)$−4s mixing is allowed, the repulsion between such *close* orbitals makes it that, in $K_2MgF_4:Ni^+$, the $a_{1g}^*(\sim 3z^2 - r^2)$ orbital is lying *below* $b_{1g}^*(\sim x^2 - y^2)$ when $R_{eq} = R_{ax}$, thus favoring an elongated geometry.[25]

In conclusion, it has been shown that the small distortion in the *model* system $K_2ZnF_4:Cu^{2+}$ is not due to a JT effect but to a vibronic coupling with two symmetric a_{1g} modes, which does not give rise to any symmetry breaking of the CuF_6^{4-} complex subject to the internal field of the host lattice. Further work on the influence of internal fields upon the structure of insulating compounds containing d^9 ions is currently in progress.

AUTHOR INFORMATION

Corresponding Author

*E-mail: aramburj@unican.es.

Notes

The authors declare no competing financial interest.

dx.doi.org/10.1021/ic400105z | Inorg. Chem. 2013, 52, 6923−6933

■ ACKNOWLEDGMENTS

The support by the Spanish Ministerio de Ciencia y Tecnología under Projects FIS2012-30996 and FIS2009-07083 is acknowledged

■ REFERENCES

(1) Garcia-Fernandez, P.; Aramburu, J. A.; Barriuso, M. T.; Moreno, M. *J. Phys. Chem. Lett.* **2010**, *1*, 647−651.
(2) Babel, D.; Tressaud, A. *Inorganic Solid Fluorides*; Hagenmuller, P., Ed.; Academic Press: New York, 1985; p 77.
(3) Garcia-Fernandez, P.; García-Lastra, J. M.; Trueba, A.; Barriuso, M. T.; Aramburu, J. A.; Moreno, M. *Phys. Rev. B* **2012**, *85*, 094110−1−9.
(4) Riley, M.; Hitchman, M. A.; Reinen, D.; Steffen, G. *Inorg. Chem.* **1988**, *27*, 1924−1934.
(5) Spaeth, J. M.; Koschnick, F. *J. Phys. Chem. Solids* **1991**, *52*, 1−34.
(6) Breñosa, A. G.; Moreno, M.; Rodriguez, F.; Couzi, M. *Phys. Rev. B* **1991**, *44*, 9859−9863.
(7) Bill, H. *The Dynamical Jahn-Teller Effect in Localized Systems*; Perlin, Yu. E; Wagner, M.; Elsevier: Amsterdam, 1984.
(8) Bersuker, I. B. *The Jahn-Teller Effect*; Cambridge University Press: Cambridge, U. K., 2006.
(9) Minner, E.; Lovy, D.; Bill, H. *J. Chem. Phys.* **1993**, *99*, 6378−6383.
(10) Minner, E. Thesis, Université de Geneve, Geneva, Switzerland, 1993, p 70
(11) Reinen, D.; Krause, S. *J. Am. Chem. Soc.* **1981**, *20*, 2750−2759.
(12) Hitchman, M. A.; McDonald, R. G.; Reinen, D. *Inorg. Chem.* **1986**, *25*, 519−522.
(13) Riley, M. J.; Dubicki, L.; Moran, G.; Krausz, E. R. *Chem. Phys.* **1990**, *14*, 363−373.
(14) Dubicki, L.; Riley, M. J.; Krausz, E. R. *J. Chem. Phys.* **1994**, *101*, 1930−1939.
(15) Reinen, D. *Inorg. Chem.* **2012**, *51*, 4458−4472.
(16) García-Fernández, P.; Bersuker, I. B.; Aramburu, J. A.; Barriuso, M. T.; Moreno, M. *Phys. Rev. B* **2005**, *71*, 184117−1−10.
(17) Herdtweck, E.; Babel, D. *Z. Kristallogr.* **1980**, *153*, 189−199.
(18) Garcia-Lastra, J. M.; Barriuso, M. T.; Aramburu, J. A.; Moreno, M. *Chem. Phys. Lett.* **2009**, *473*, 88−91.
(19) Grochala, W.; Hoffman, R. *Angew. Chem., Int. Ed.* **2001**, *40*, 2743−2781.
(20) Kimura, T.; Tokura, Y. *Annu. Rev. Mater. Sci.* **2000**, *30*, 451−474.
(21) Keller, H.; Bussmann-Holder, A.; Müller, K. A. *Mater. Today* **2008**, *11*, 38−46.
(22) Goodenough, J. B. *Annu. Rev. Mater. Sci.* **1998**, *28*, 1−27.
(23) Halcrow, M. A. *Chem. Soc. Rev.* **2013**, DOI: 10.1039/C2CS35253B.
(24) Babel, D.; Herdtweck, E. *Z. Anorg. Allg. Chem.* **1982**, *487*, 75−84.
(25) Garcia-Lastra, J. M.; Aramburu, J. A.; Barriuso, M. T.; Moreno, M. *Phys. Rev. Lett.* **2004**, *93*, 226402−1−4.
(26) Narayana, P. A. *Phys. Rev. B* **1974**, *10*, 2676−2680.
(27) Folen, V. J. *Phys. Rev. B* **1972**, *6*, 1670−1677.
(28) Yamaguchi, Y. *Solid State Commun.* **1972**, *11*, 1611−1614.
(29) Moreno, M.; Barriuso, M. T.; Aramburu, J. A.; Garcia-Fernandez, P.; Garcia-Lastra, J. M. *J. Phys.: Condens. Matter* **2006**, *18*, R315−R360.
(30) CRYSTAL basis sets. http://www.crystal.unito.it/Basis_Sets/Ptable.html.
(31) Bilc, D. I.; Orlando, R.; Shaltaf, R.; Rignanese, G.-M.; Iñiguez, J.; Ghosez, Ph. *Phys. Rev. B* **2008**, *77*, 165107−1−13.
(32) te Velde, G.; Bickelhaupt, F. M.; Baerends, E. J.; Guerra, C. F.; van Gisbergen, S. J. A.; Snijders, J. D.; Ziegler, T. *J. Comput. Chem.* **2001**, *22*, 931−967.
(33) Perdew, J. P. *Electronic Structure of Solids '91*; Ziesche, P., Eschrig, H., Eds.; Akademie Verlag: Berlin, 1991; p 11.
(34) Aramburu, J. A.; García-Lastra, J. M.; Barriuso, M. T.; Moreno, M. *Int. J. Quantum Chem.* **2003**, *91*, 197−201.
(35) Trueba, A.; Garcia-Fernandez, P.; García-Lastra, J. M.; Aramburu, J. A.; Barriuso, M. T.; Moreno, M. *J. Phys. Chem A* **2011**, *115*, 1423−1432.
(36) Ham, F. S. *Electron Paramagnetic Resonance*; Geschwind, S., Ed.; Plenum: New York, 1972; p 1.
(37) Boatner, L. A.; Reynolds, R. W.; Abraham, M. M.; Chen, Y. *Phys. Rev. Lett.* **1973**, *31*, 7−10.
(38) Riley, M. J.; Noble, C. J.; Tregenna-Piggott, P. L. W. *J. Chem. Phys.* **2009**, *130*, 104708−1-14.
(39) Garcia-Fernandez, P.; Trueba, A.; Barriuso, M. T.; Aramburu, J. A.; Moreno, M. *Phys. Rev. Lett.* **2010**, *104*, 035901−1−4.
(40) Garcia-Fernandez, P.; Trueba, A.; Barriuso, M. T.; Aramburu, J. A.; Moreno, M. *Vibronic Interactions and the Jahn−Teller Effect*; Daul, C., Atanasov, M., Tregenna-Piggott, P. L. W., Eds.; Springer-Verlag: Heidelberg, Germany, 2012; p 105.
(41) Ballhausen, C. J. *Ligand Field Theory*, McGraw-Hill: New York, 1962; p 73.
(42) Barriuso, M. T.; Garcia-Fernandez, P.; Aramburu, J. A.; Moreno, M. *Solid State Commun.* **2001**, *120*, 1−5.
(43) Hayes, W.; Wilkens, J. *Proc. R. Soc. London, Ser. A* **1964**, *281*, 340−361.
(44) McLain, S. E.; Dolgos, M. R.; Tennant, D. A.; Turner, J. F. C.; Barnes, T.; Proffen, T.; Sales, B. C.; Bewley, R. I. *Nat. Mater.* **2006**, *5*, 561−566.
(45) Barriuso, M. T.; Aramburu, J. A.; Moreno, M. *J. Phys.: Condens Matter* **1990**, *2*, 771−777.
(46) Nurullin, G. M.; Galygo, L. N.; Egranov, A. V.; Nepomnyachikh, A. I. *J. Phys.: Condens Matter* **1991**, *3*, 83−90.
(47) Shengelaya, A.; Drulis, H.; Macalik, B.; Suzynska, M. *Z. Phys. B* **1996**, *101*, 373−376.
(48) Zorita, E.; Alonso, P. J.; Alcala, R. *Phys. Rev. B* **1987**, *35*, 3116−3121.
(49) Villacampa, B.; Alcala, R.; Alonso, P. J.; Moreno, M.; Barriuso, M. T.; Aramburu, J. A. *Phys. Rev. B* **1994**, *49*, 1039−1047.
(50) Riley, M. J.; Hitchman, M. A.; Reinen, D. *Chem. Phys.* **1986**, *102*, 11−28.
(51) Dubicki, L.; Krausz, E. R.; Riley, M. J.; Yamada, I. *Chem. Phys. Lett.* **1989**, *157*, 315−320.
(52) Garcia-Fernandez, P.; Sousa, C.; Aramburu, J. A.; Barriuso, M. T.; Moreno, M. *Phys. Rev. B* **2005**, *72*, 155107−1−5.
(53) Vercammen, H.; Schoemaker, D.; Briat, B.; Ramaz, F.; Callens, F. *Phys. Rev. B* **1999**, *59*, 286−292.
(54) Garcia-Fernandez, P.; Barriuso, M. T.; Aramburu, J. A.; Moreno, M. *Chem. Phys. Lett.* **2003**, *374*, 151−156.
(55) Garcia-Lastra, J. M.; Barriuso, M. T.; Aramburu, J. A.; Moreno, M. *Phys. Rev. B* **2005**, *72*, 113104−1−4; *ibid.* **2006**, *74*, 115118−1−5.
(56) Aramburu, J. A.; Garcia-Fernandez, P.; Garcia-Lastra, J. M.; Barriuso, M. T.; Moreno, M. *Phys. Rev. B* **2012**, *85*, 245118−1−10.
(57) Trueba, A.; Garcia-Lastra, J. M.; Garcia-Fernandez, P.; Barriuso, M. T.; Aramburu, J. A.; Moreno, M. *J. Phys. Chem A* **2011**, *115*, 13399−13406.
(58) Takeuchi, H.; Arakawa, M.; Aoki, H.; Yosida, T.; Horai, K. *J. Phys. Soc. Jpn.* **1982**, *51*, 3166−3172.
(59) Garcia-Lastra, J. M.; Barriuso, M. T.; Aramburu, J. A.; Moreno, M. *J. Phys.: Cond. Matter* **2010**, *22*, 155502−155509.
(60) Sierro, J. *J. Phys. Chem. Solids* **1966**, *28*, 417−422.
(61) Trueba, A.; Garcia-Lastra, J. M.; De Graaf, C.; Garcia-Fernandez, P.; Barriuso, M. T.; Aramburu, J. A.; Moreno, M. *Chem. Phys. Lett.* **2006**, *430*, 51−55.
(62) Halder, G. J.; Chapmam, K. W.; Schlueter, J. A.; Manson, J. L. *Angw. Chem., Int. Ed.* **2011**, *50*, 419−421.
(63) Ulanov, V. A.; Krupski, M.; Hoffmann, S. K.; Zaripov, M. M. *J. Phys.: Condens. Matter* **2003**, *15*, 1081−1096.
(64) Garcia-Fernandez, P.; Aramburu, J. A.; Barriuso, M. T.; Moreno, M. *Phys. Rev. B* **2004**, *69*, 174110−1−8.
(65) Kohn, W. *Phys. Rev. Lett.* **1996**, *76*, 3168−3171.
(66) Resta, R. *J. Phys.: Cond. Matter* **2002**, *14*, R625−R656.

(67) Alcalá, R.; Zorita, E.; Alonso, P. J. *J. Phys C: Solid State Phys.* **1988**, *21*, 461−470.